Academic Journal of Science and Technology
ISSN: 2771-3032 | Vol. 5, No. 3, 2023

Deformation Analysis of Guobu Slope based on SBAS-InSAR

Conghua Li*, Long Li, Chonghui Zhang

School of Geomatics and Urban Spatial Informatics, Beijing University of Civil Engineering and Architecture, Beijing 102616, China
* **Corresponding author**

Abstract: The Laxiwa hydropower station reservoir in the upper reaches of the Yellow River basin is located in a canyon zone. Due to its complex terrain and difficult transportation, traditional monitoring methods are difficult to implement in this area, especially during the critical deformation stage when personnel may face danger or encounter difficulty reaching the site. To achieve long-term continuous dynamic monitoring of the upstream active slope of the Laxiwa hydropower station, namely the Guobu slope, SBAS-InSAR technology has been adopted as a replacement for traditional measurement methods to monitor landslide movements. Based on the deformation information of the monitoring targets, safety analysis, and disaster warnings are conducted to ensure the safe operation of the power station and the safety of downstream communities and residents' lives and property.

Keywords: SBAS-InSAR, Laxiwa hydropower station, Guobu slope, Displacement monitoring, Deformation analysis.

1. Introduction

Landslides are one of the most frequent and hazardous geological disasters worldwide, with high degree of concealment and destructiveness, posing significant threats to people's lives, property safety, and infrastructure security[1]. The surface deformation of landslide is the most direct source of physical information to analyze the stability and danger of landslide, which is of great significance for the early identification and long-term monitoring of large-scale landslides[2],[3].

Currently, monitoring techniques for landslide surface deformation mainly fall into two categories: contact and non-contact monitoring techniques[4]. Contact monitoring techniques include precision level survey and Global Navigation Satellite System (GNSS). Due to their high monitoring accuracy, precise leveling and GNSS technologies have been widely used for surface deformation monitoring of landslides. However, these methods have a single-point monitoring mode, low spatial resolution, limited monitoring range, and are easily affected by topographical factors. In addition, instrument deployment and field measurements require significant human and material resources, making it difficult to achieve continuous and full coverage monitoring of large and complex terrain areas. The non-contact deformation monitoring mainly uses UAV remote sensing, Light Detection and Ranging (LiDAR), Ground-Based Synthetic Aperture Radar (GB-SAR), satellite-borne optical remote sensing, and satellite-borne synthetic aperture radar. Unmanned aerial vehicle remote sensing has flexible application scenarios and simple operation, which is suitable for emergency response and real-time evaluation of landslide disasters. However, its platform stability is poor, imaging range is small, and it is easily affected by external weather and terrain conditions. LiDAR and GB-SAR have high observation frequency, which can achieve continuous observation with high precision and high spatial resolution. However, they have a small monitoring range and are only suitable for deformation monitoring of individual landslides. Satellite-borne optical remote sensing has good periodicity, large data volume, and wide coverage, which can achieve dynamic monitoring of landslides on a large scale. However, its monitoring accuracy is low and cannot identify potential landslides with slow deformation, and it is easily affected by climate conditions such as clouds, fog, and rain. Satellite-borne synthetic aperture radar, as an active microwave imaging technology that combines signal theory and interferometry, can obtain ground image data around the clock. Synthetic Aperture Radar Interferometry (InSAR) technology uses two or more SAR images of the same area at different times for interferometric processing, and the deformation data obtained has high precision, high spatial resolution, high revisit frequency, wide coverage, and is less affected by weather conditions. It has become an important means for monitoring landslide deformation[5],[6].

The satellite-borne synthetic aperture interferometry (InSAR) can acquire surface deformation information of the Earth with centimeter or even millimeter accuracy, and has been widely used in earthquake, volcano, surface deformation monitoring and early identification of landslide[7]–[9]. Su et al. utilized SBAS-InSAR technology to process 150 Sentinel 1-A images in the year 2017, and identified 762 landslides along the China-Pakistan Highway, including 57 complex landslides, 126 rockfalls, 167 debris slides, and 412 unstable slopes. They conducted a detailed analysis of the landslide classification, displacement characteristics, spatial distribution, and the relationship with various influencing factors[10]. Li et al. utilized Sentinel-1 SAR data from October 2014 to June 2022 to extract the deformation rate and annual maximum deformation area changes of landslides around the Xiluodu Reservoir. Based on the deformation characteristics of the landslides, they classified them into three regions and analyzed the impact of the reservoir water level on the contribution of the landslides[11]. In this paper, a total of 103 scenes of Sentinel-1 data between September 2015 and December 2019 were used to obtain the surface deformation results of the Laxiwa hydropower plant region based on SBAS-InSAR technology, and the regional deformation results were correlated with the landslide development characteristics to extract the long-term

deformation characteristics of the Guobu slope landslide in the region, which provides an important reference for regional landslide disaster prevention and control and safety warning.

2. Study area and Materials

(1) Study area

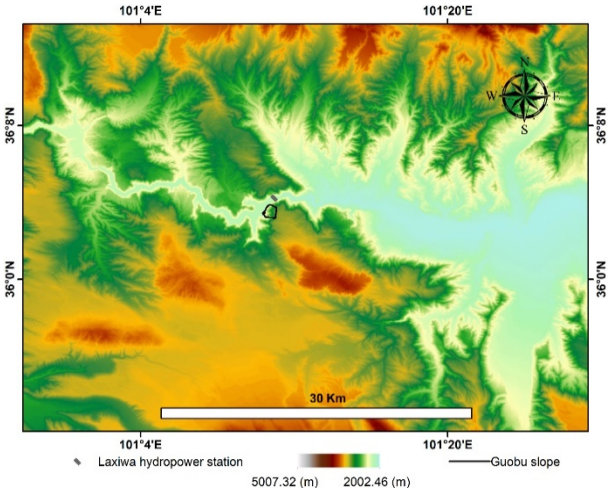

Figure 1. Overview of the study area

The upstream of the Yellow River is located in the transition zone between the first and second order terrain in China, with large topographic relief. The abundant water resources and the huge topographic drop mean that the water resources in the region contain great energy. At the same time, the river valley in this region is mainly composed of hard rock bodies such as granite and shallow metamorphic rocks, which have excellent geological engineering properties for dam building. The Laxiwa hydropower station, the second cascade power station from Longyang Gorge to Qingtong Gorge in the Yellow River Basin, is located approximately 32 kilometers downstream of the Longyang Gorge reservoir outlet, 4.5 kilometers from the town of Laxiwa, and 26 kilometers from the county seat of Guide. The elevation of the mountain tops on either side of the Yellow River channel in the reservoir area generally ranges from 2,000 to 4,200 meters, with a relative height difference of 700 to 2,200 meters, as shown in Figure 1. The valley in the reservoir area is often deeply cut and forms a "V"-shaped canyon, which is a typical high mountain canyon landform with a winding and tortuous river channel. In March 2009, the Laxiwa hydropower station began storing water. In May of the same year, staff discovered that the Guobu slope that located upstream of the hydropower station had experienced displacement and deformation. This posed a significant threat to the safe operation of the hydropower station and the personal and property safety of residents in the downstream community 4 kilometers away. Therefore, this region was selected as the study area, which is worthy of people's attention.

(2) Materials

In this paper, we select single look complex (SLC) images from IW mode as the data source, the number of SAR images is 103 views, the polarization mode VV, the time scale is from September 20, 2015 to December 28, 2019, the shortest time interval is 12 days. The main parameters of the SAR images are listed in Table 1. Due to the northwest-facing (NW285°) slope of Guobu slope with an average slope angle of 43°, the radar pulse beam of the ascending orbit first reaches the top of the slope and then reaches the foot of the slope, causing echoes from different areas to be projected into the same SAR image unit, resulting in a phenomenon known as layover. Therefore, descending orbit data is the only viable choice to realize InSAR monitoring of Guobu slope.

Table 1. Sentinel-1 SAR image parameters.

Orbit	Descending
Beam mode	IW
Repeat period(d)	12
Resolution (Rg×Az m)	2.3×13.9
Heading Angle (°)	193.1
Incidence Angle (°)	32.6

In order to eliminate and attenuate the phase errors caused by orbital errors, this paper selects POD precision orbit ephemeris data with positioning accuracy better than 5 cm to correct the satellite orbit data, which can be downloaded from the website of ESA's Copernicus Earth Observation data center (https://scihub.copernicus.eu/gnss/#/home). The DEM data plays a crucial role in the processing of the SBAS-InSAR technology, as it can be utilized for the coregistration of SAR imagery, the removal of topographic phases from interferograms, and the estimation and correction of atmospheric delays. Therefore, this paper has selected the 30-meter resolution COP (Conpernicus) DEM data, which can precisely provide elevation data for the study area and enhance the reliability of the SBAS-InSAR results, It is possible to obtain it through the OpenTopography website (https://portal.opentopography.org/datasets).

3. SBAS-InSAR Data Processing

The Small Baseline Subset InSAR (SBAS-InSAR) technique was first proposed by Berardino and Lanari et al.[12]. This method obtains a series of short spatial baseline differential interferograms by combining data, which can better overcome spatial de-correlation. The SBAS-InSAR technique uses singular value decomposition (SVD) to solve deformation rates, connecting isolated SAR data that are separated by larger spatial baselines to further increase the temporal sampling rate of the observation data[13]. This method can effectively mitigate atmospheric effects, reduce phase noise and errors[10]. Discussion on the principles of SBAS-InSAR technology has been established in nu-merous articles and will not be elaborated further in this paper. For further information, please refer to the citations [12], [14], and [15] in the reference list.

The data processing procedure entails the following steps: 1) Generating a baseline connectivity graph. Due to the complex topography and proximity to the river in the study area, the spatial baseline threshold is set to 200m and the temporal baseline threshold to 60 days. This is done to construct a connectivity graph that generates corresponding interferograms, and to combine interferograms with spatial baselines smaller than the critical baseline, show in Figure 2. 2) Performing differential interferometric processing. The data acquired on July 11, 2017 is selected as the master image. The other images are coregistered to this image to generate interferograms. COP DEM data and corresponding precision orbit data are used to remove the flat phase, and Goldstein and Minimum Cost Flow (MCF) filtering and phase unwrapping are applied to produce a series of phase images. Setting the unwrapping threshold to 0.2, the pixels with coherence below

0.2 will not be included in the subsequent calculations 3) Eliminating the constant phase and phase jumps from the phase images. 4) Utilizing Singular Value Decomposition (SVD) matrix inversion technique to obtain the deformation rate for the first time. 5) Applying spatial domain high-pass filtering and temporal domain low-pass filtering to the residual phase to remove atmospheric phase and obtain a more accurate time-series deformation rate with filtering windows set to 1000m and 365 days respectively. 6) Geocoding. The deformation results are transformed from slant-range projection to geographic coordinate projection to obtain the final deformation rate in the mapping reference system.

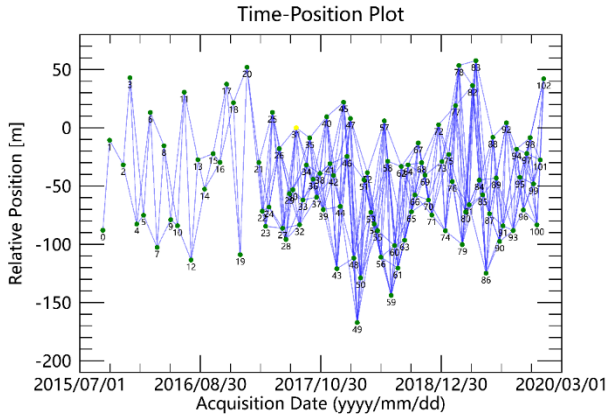

Figure 2. Thetime-temporal baseline plot of Sentinel-1 images.

4. Guobu Slope Surface Deformation Analysis

Using the SBAS-InSAR technique and Sentinel-1 data, the surface deformation information of the Laxiwa Hydropower Station area was obtained for a period of five years. The deformation results were visualized and analyzed using ArcGIS software, overlaid on satellite maps as shown in Figure 3. Negative values indicate that the direction of movement of ground targets is away from the satellite (i.e., subsidence), while positive values indicate that the direction of movement is towards the satellite (i.e., uplift). From the figure, it can be seen that, except for the lack of deformation monitoring results in water bodies and SAR image overlapping areas, shadow areas, and perspective contraction areas, most areas within the study area have good spatial continuity of deformation monitoring results, which can fully demonstrate the ground movement status and slope stability within the Laxiwa Hydropower Station area during the monitoring period. To better analyze the stability of the study area, the deformation information was extracted from the annual average deformation rate map and counted to create a histogram of the deformation rate and the corresponding number of pixels, as shown in Figure 4. It was found that a total of 346,343 valid pixels were monitored in this study, and about 94.36% of the pixels had deformation rates between −5 and 5 mm/yr, indicating small deformation and stable conditions in most areas of the study area. The number of uplift pixels with deformation rates greater than 5 mm/yr was 10,416, accounting for 2.9% of the total, and their distribution was relatively scattered. The number of subsidence pixels with deformation rates less than −5 mm/yr was 9,653, accounting for 2.7% of the total, and they were concentrated within the range defined by the blue solid line in Figure 4, which is the area where the Guobu slope is located.

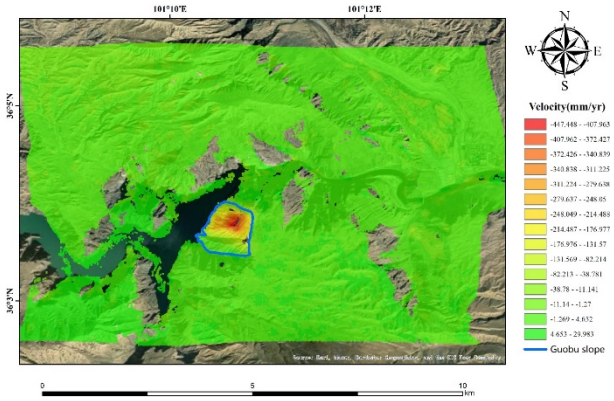

Figure 3. Average annual deformation rate in the study area

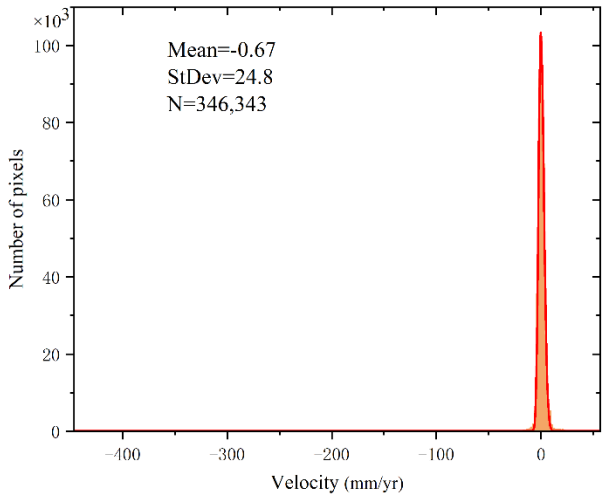

Figure 4. Histogram of the number of pixels and the velocity of deformation

(1) Spatial characteristics of the deformation of the Guobu slope

From the deformation results shown in Figure 4, it can be seen that there is significant deformation displacement on the Guobu slope in the study area, which poses a huge threat to downstream Laxiwa hydropower station and local residents. Therefore, the focus will be on analyzing the spatiotemporal characteristics, motion laws, and responses to external driving factors of the Guobu slope deformation. In terms of space, the cumulative deformation and average deformation rate of selected time points were extracted from the deformation results obtained by SBAS-InSAR technology to study the deformation characteristics of the Guobu slope, as shown in Figure 6. Figure 6a shows the spatial variation of the deformation rate of the Guobu slope from September 2015 to December 2019, and Figure 6b shows the cumulative deformation of the Guobu slope at selected time points with September 20, 2015 as the zero deformation reference. It can be seen that the maximum deformation rate of the Guobu slope reached -447.448 mm/yr during the monitoring period, and the maximum cumulative deformation was -1860 mm. There is an obvious boundary between the landslide rear and the stable area, corresponding to a clear tearing edge on the top platform of the Google Earth optical image in Figure 3 1e. The left and right edges are defined by two gullies, and the overall direction of landslide movement is NW285°. The projection of the deformation area on the plane shows a funnel

shape with obvious landslide walls, steps, and rear cracks. It can be seen from Figure 6 that the boundary of the landslide is obvious, and the landslide area did not expand significantly from June 10, 2016 to December 28, 2019, indicating that the movement of the Guobu slope is integral.

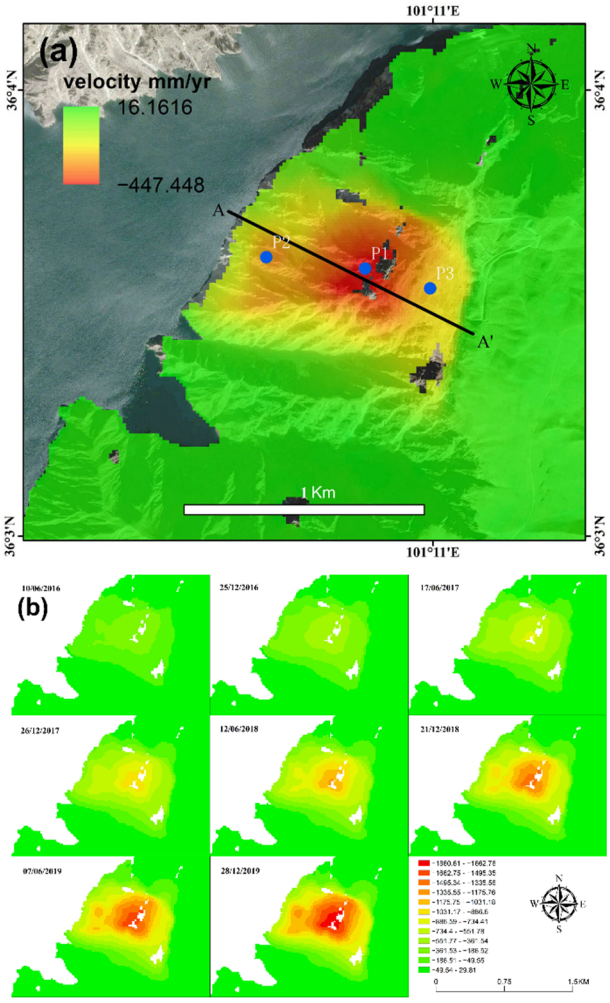

Figure 5. Deformation velocity and cumulative deformation of Guobu slope

In order to further investigate the spatial characteristics of the deformation of Guobu slope, a profile line A-A' was drawn along the main sliding direction of the landslide body, from the top of the slope to the foot of the slope, as shown by the black line in Figure 5a. Then, the deformation rate and elevation values of all pixels on the profile line were extracted and displayed in the form of a line chart, resulting in an overlay of deformation rate and elevation along the profile line, as shown in Figure 6. The blue line in Figure 6 represents the elevation variation of pixels along the profile line AA', while the red line represents the deformation rate of pixels along the profile line. The green dashed line corresponds to the design water level elevation of 2452 meters, and the black dashed line is the auxiliary line that determines the elevation of the severely deformed area. It can be seen that during the stable operation of Laxiwa, the altitude difference from the water surface to the top of Guobu slope reaches 500m. The severe deformation area with an annual average deformation rate exceeding −400mm/yr is located in the middle and upper part of the slope, between the elevations of 2700~2850m. In addition, the annual average deformation rate of the entire slope exceeds −200mm/yr. The deformation rates of various parts of the landslide show a certain spatial difference. The upper part near the edge of the top platform has a higher deformation rate, while the deformation rate of the foot and platform area is roughly the same. The deformation rate shows a "V"-shaped change from slow to fast and then to slow again from the top to the bottom of the slope. The deformation rate of the slope surface exhibits a typical nonlinear spatiotemporal distribution.

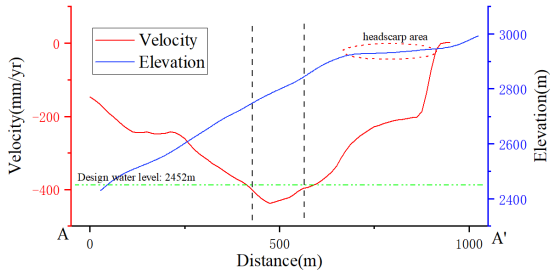

Figure 6. Profiles of deformation rate and elevation

(2) Temporal characteristics of the deformation of the Guobu slope.

We conducted a time-series analysis of three different target points on the slope surface, as indicated by the blue dots in Figure 5a. To mitigate the interference of random errors on these selected points, we established a 60-meter buffer zone around each target point. The average displacement of all deformation points within the buffer zone was taken as the time-series deformation data for each target point, as shown in Figure 7, where the error bars represent the standard deviation of all measurement values within the buffer zone. During the monitoring period, the cumulative deformation of the P1 point located in the upper-middle part of the landslide exceeded 1.75 meters, while that of the P2 point located at the bottom of the landslide was about 1.2 meters, and the cumulative deformation of the P3 point in the central area of the platform was close to 1 meter. The slope of the deformation time series in the figure represents the deformation rate, and it can be observed that the deformation rates of the three target points remained stable over the entire study period, with fluctuations occurring only in the short term and small range. It can be concluded that the deformation characteristics of Guobu slope vary at different time scales. In the short term (weeks or even months), the slope deformation is influenced by external factors such as rainfall and water level changes, leading to apparent acceleration or deceleration. In the long term (annual cycle), the slope deformation is mainly affected by geological structures and surface gravity.

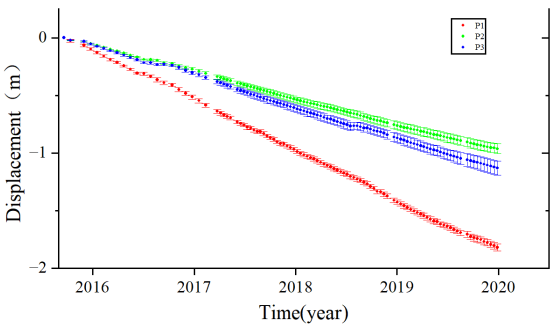

Figure 7. Time series of deformation feature points

(3) Correlation of SBAS-InSAR results with precipitation

As the water level of the Laxiwa Hydropower Station reservoir remained stable at the designed level of 2452m during the monitoring period, our primary focus was on the relationship between deformation and precipitation. During the period from September 2015 to December 2019, the deformation time series of characteristic points exhibited an uneven linear variation, which can be considered as an arithmetic sum of linear and nonlinear components. The linear component represents the non-elastic displacement of the slope caused by its own gravity, while the nonlinear component represents the displacement acceleration or deceleration caused by external factors. In this paper, the linear component of deformation was obtained by the method of least squares fitting, while the nonlinear component was defined as the difference between the deformation time series and the linear component. A relationship graph was constructed between the displacement nonlinear component and the down-sampled precipitation and water level data, as shown in Figure 8. It was found that the non-linear deformation amplitude changes in the high-altitude area of the platform edge P1 and the low-altitude area of the slope foot P2 were comparable (−20mm-30mm), while the non-linear deformation amplitude in the platform area P3 was smaller (−15mm-20mm), indicating that the top platform was less affected by external factors and more stable. By analyzing the joint response of non-linear deformation and external precipitation and reservoir water level, it was found that the four amplitudes of P1 had a good response to precipitation and reservoir water level; P2 and P3 only showed a certain amplitude response change in January 2016 to March 2017 and June 2018 to March 2019. The relationship between the images can only qualitatively indicate that the deformation of Guobu slope is affected by precipitation and water level, and there is a certain lag.

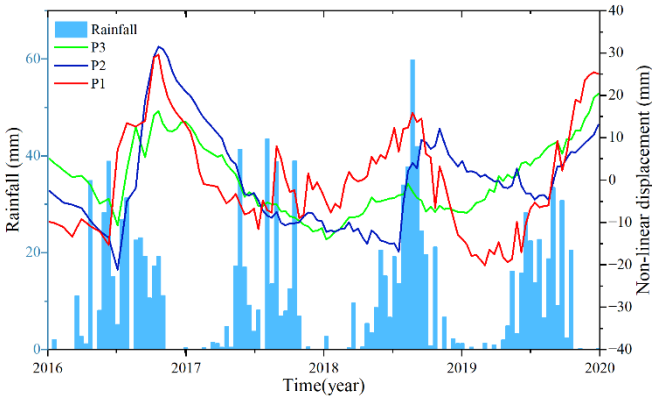

Figure 8. Precipitation and non-linear displacement of InSAR deformation

5. Conclusions

This paper employed the SBAS-InSAR technique to process 103 Sentinel-1 image data from September 2015 to December 2020 at the Laxiwa Hydropower Station, analyzing and monitoring the spatiotemporal evolution characteristics of ground subsidence at the Guobu Slope. The following conclusions were drawn:

1) The results of SBAS-InSAR deformation show that the Guobu slope is in a continuous state of motion, with the highest deformation rate in the high area, with a cumulative deformation of up to 1.7m. Once the landslide is destabilized, it will block the Yellow River and create large-scale waves, posing a serious threat to the normal operation of the hydropower station and the normal production and life of downstream communities. Therefore, it is recommended that this area be continuously monitored and measures be taken to mitigate the deformation.

2) The high level deformation of Guobu slope exhibits typical toppling damage, and the foot of the slope shows creep-slip deformation state. Geological structure and gravitational forces exert a controlling influence on landslides, manifested in their impact on the shape of the landslide body, the location of material accumulation, and the initiation area, etc. Rainfall serves as a inducing factor in the development of landslides. It does so by augmenting the weight of landslides and diminishing their cohesion, ultimately inducing them. The acceleration in the deformation of landslides, provoked by rainfall, experiences a certain degree of delay.

Reference

[1] Alessandro Cesare Mondini, Fausto Guzzetti, Kang-Tsung Chang, et al. Landslide failures detection and mapping using Synthetic Aperture Radar: Past, present and future[J/OL]. Earth-Science Reviews, 2021, 216: 103574. DOI:10.1016/j.earscirev.2021.103574.

[2] Tingchen Wu, Xiao Xie, Haoyu Wu, et al. A Quantitative Analysis Method of Regional Rainfall-Induced Landslide Deformation Response Variation Based on a Time-Domain Correlation Model[J/OL]. Land, 2022, 11(5): 703. DOI:10.3390/land11050703.

[3] Xiaojie Liu. Research on key technologies for early identification, monitoring and forecasting of wide-area landslides with spaceborne radar remote sensing[D/OL]. Universidad de Alicante, 2022[2023-03-14]. https://kns.cnki.net/kcms/detail/detail.aspx?FileName=1023419818&DbName=CDFDTEMP&DbCode=CDFD.

[4] Jianming Kuang, Linlin Ge, Alex Hay-Man Ng, et al. Detection and Deformation Characterization of the 2020 Aniangzhai Landslide Using Time-Series Insar and Optical Datasets[C/OL]//2021 IEEE International Geoscience and Remote Sensing Symposium IGARSS. Brussels, Belgium: IEEE, 2021: 6595-6598[2022-12-08]. https://ieeexplore.ieee.org/document/9554326/. DOI:10.1109/IGARSS47720.2021.9554326.

[5] Yan Yan, Yong Wang. Determining Suitable Spaceborne SAR Observations and Ground Control Points for Surface Deformation Study in Rugged Terrain With InSAR Technique[J/OL]. IEEE Journal of Selected Topics in Applied Earth Observations and Remote Sensing, 2021, 14: 11324-11334. DOI:10.1109/JSTARS.2021.3123326.

[6] Bingli Hu, Lijun Su, Bo Zhao, et al. New Insight into the Sliding Mechanism and Post-Stability of the 2017 Xinmo Landslide in Sichuan, China[J/OL]. Bulletin of Engineering Geology and the Environment, 2022, 81(10): 430. DOI:10.1007/s10064-022-02917-3.

[7] Bayer B, Simoni A, Schmidt D, et al. Using advanced InSAR techniques to monitor landslide deformations induced by tunneling in the Northern Apennines, Italy[J/OL]. Engineering Geology, 2017, 226: 20-32. DOI:10.1016/j.enggeo.2017.03.026.

[8] Houjun Jiang, Guangcai Feng, Teng Wang, et al. Toward full exploitation of coherent and incoherent information in Sentinel-1 TOPS data for retrieving surface displacement: Application to the 2016 Kumamoto (Japan) earthquake: FULL EXPLOITATION OF SENTINEL-1 TOPS DATA[J/OL]. Geophysical Research Letters, 2017[2023-02-20].

http://doi.wiley.com/10.1002/2016GL072253. DOI:10.1002/2016GL072253.

[9] Guzalay Sataer, Mohamed Sultan, Mustafa Kemal Emil, et al. Remote Sensing Application for Landslide Detection, Monitoring along Eastern Lake Michigan (Miami Park, MI)[J/OL]. Remote Sensing, 2022, 14(14): 3474. DOI:10.3390/rs14143474.

[10] Xiaojun Su, Yi Zhang, Xingmin Meng, et al. Updating Inventory, Deformation, and Development Characteristics of Landslides in Hunza Valley, NW Karakoram, Pakistan by SBAS-InSAR[J/OL]. Remote Sensing, 2022, 14(19): 4907. DOI:10.3390/rs14194907.

[11] Lingjing Li, Xin Yao, Baoping Wen, et al. The long-term failure processes of a large reactivated landslide in the Xiluodu reservoir area based on InSAR technology[J/OL]. Frontiers in Earth Science, 2023, 10: 1055890. DOI:10.3389/feart.2022.1055890.

[12] P. Berardino, G. Fornaro, R. Lanari, et al. A new algorithm for surface deformation monitoring based on small baseline differential SAR interferograms[J/OL]. IEEE Transactions on Geoscience and Remote Sensing, 2002, 40(11): 2375-2383. DOI:10.1109/TGRS.2002.803792.

[13] Jiaming Yao, Xin Yao, Xinghong Liu. Landslide Detection and Mapping Based on SBAS-InSAR and PS-InSAR: A Case Study in Gongjue County, Tibet, China[J/OL]. Remote Sensing, 2022, 14(19): 4728. DOI:10.3390/rs14194728.

[14] Ming Chang, Wenjing Sun, Hengzhi Xu, et al. Identification and deformation analysis of potential landslides after the Jiuzhaigou earthquake by SBAS-InSAR[J/OL]. Environmental Science and Pollution Research, 2023[2023-02-18]. https://link.springer.com/10.1007/s11356-022-25055-5. DOI:10.1007/s11356-022-25055-5.

[15] Zhang P, Guo Z, Guo S, et al. Land Subsidence Monitoring Method in Regions of Variable Radar Reflection Characteristics by Integrating PS-InSAR and SBAS-InSAR Techniques[J]. Remote Sensing, 2022, 14(14): 3265.